Effects of pore geometry on flowing foam dynamics in 3D printed porous media

Kofi Osei-Bonsu[1], Paul Grassia[2,3] and Nima Shokri*[1]

[1]School of Chemical Engineering and Analytical Science, University of Manchester, Manchester, UK

[2] Department of Chemical and Process Engineering, University of Strathclyde, Glasgow, UK

*Corresponding author

Dr. Nima Shokri

School of Chemical Engineering and Analytical Science

Room C26, The Mill

The University of Manchester

Sackville Street, Manchester, M13 9PL, UK

Tel: 0441613063980

Email: nima.shokri@manchester.ac.uk

Group website: http://personalpages.manchester.ac.uk/staff/nima.shokri/

Abstract

Foam flow in porous media is important in several environmental and industrial applications including soil remediation and enhanced oil recovery. The behaviour of foam is greatly influenced by transport properties of porous media, properties of foam and the fluid residing in porous media. We conducted a series of experiments to investigate the effects of pore geometry on foam flow in porous media and its implications for hydrocarbon displacement. We fabricated four porous media with well-defined pore throat size distributions, permeability and angularity by means of 3D printing technology. The models were initially saturated with oil. Gas and surfactant solution were subsequently injected into the model simultaneously for in-situ generation of foam to displace the oil. Displacement dynamics were recorded using an automatedie imaging setup. Analysis of the pore-scale images revealed that the injected pore volumes required for the initiation of foam generation decreased as the pore size of porous media increased, presumably due to the lower entry capillary pressure. For the same pore throat size range, changes in the permeability due to increased number of pore throats did not appear to have a significant influence on the overall recovery of oil. Our results illustrate the impact of grain angularity on foam generation owing to its influence on the pore-to-throat aspect ratio and capillary pressure gradient.

Keywords: Foam generation and propagation in porous media, Pore geometry and angularity, Minimum pressure gradient, 3D printing technology

Introduction

Contamination of soil by non-aqueous phase liquids (NAPLs) such as hydrocarbon-based products is a major environmental concern because of the potential danger it poses to the ecosystem (Hirasaki et al., 1996; Pennell et al., 1996). In many cases, contaminants migrate downwards and eventually reach the aquifer. During this process, portions of these contaminants are trapped in smaller pores due to capillary forces, serving as a long-term source of pollution to the ground water (Hirasaki et al., 1996). Furthermore, trapped oil phases can constitute a large fraction of oil initially in petroleum reservoirs. A conventional approach to displacing this trapped phase is to inject gas or surfactant solution into the reservoir (Payatakes, 1982; Lenormand et al., 1988; Pennell et al., 1996). These methods however suffer from several drawbacks such as gravity segregation and fingering/instabilities. To overcome these deficiencies, foam flooding has been proposed as a potential solution (Schramm and Wassmuth, 1994; Jeong et al., 2000). Foam is a dispersion of gas in a liquid whereby the gas is separated by thin liquid films called lamellae. The liquid phase is generally made up of water and a foaming agent such as surfactant and/or nanoparticles to stabilize the generated lamellae and thus to improve the longevity of the bubbles (Schramm and Wassmuth, 1994; Binks and Horozov, 2005; Nguyen et al., 2014). In contrast to the sole injection of gas or surfactant solution, foam is characterised by a higher apparent viscosity, which provides a favourable mobility ratio, suppressing the formation of fingers. Moreover, the higher apparent viscosity of foam in higher permeability layers can mitigate the undesired effects of the reservoir heterogeneity by diverting flow to low permeability regions (Hirasaki and Lawson, 1985; Grassia et al., 2014; Mas-Hernandez et al., 2015).

Foam is generated in-situ by injection of alternating slugs of a surfactant solution and gas or by co-injection of surfactant and gas (Zeng et al., 2016; Osei-Bonsu et al., 2017a). Three

main foam generation mechanisms have been identified in the foam literature: snap-off, lamella division and leave behind (Ransohoff and Radke, 1988; Rossen and Gauglitz, 1990; Kovscek et al., 1994). Lamellae are created by snap-off mechanism in pore-throats when liquid gradually accumulates in gas-invaded pore throat and eventually bridges and blocks the throat (Kovscek et al., 1994; Gauglitz et al., 2002). Bubbles generated by this mechanism generally have sizes similar to the pore bodies. Snap-off is influenced by several factors including pore-to-throat aspect ratio, capillary number and pore geometry (Ransohoff and Radke, 1988; Kovscek et al., 1994). In lamella division, an existing bubble subdivides into two new bubbles upon stretching around branched points in porous media (Kovscek et al., 1994). Bubble creation by lamella division is also common when bubbles push against larger bubbles around a pore junction. The frequency of this foam generation mechanism may depend on several parameters such as the pore geometry, connectivity, and the initial size of bubbles (Kovscek et al., 1994). Foam generation by leave behind occurs when two gas menisci invade a liquid saturated pore, leaving behind a lens as the two menisci converge. A stable lens may form depending on the capillary pressure of the medium and the pressure gradient of the flow (Kovscek et al., 1994). Identifying the dominant foam generation mechanism is considered to be of importance as it can significantly influence the strength (apparent viscosity) of the foam. Foams generated by snap- off and lamella division have been observed to be stronger whereas leave behind produces weak foam (Kovscek et al., 1994).

The performance of foam as a displacement fluid in porous media is controlled by numerous parameters ranging from the physiochemical properties of the foam (i.e. gas type/composition and surfactant) (Schramm and Novosad, 1990; Andrianov et al., 2012; Zeng et al., 2016), the oil properties (Schramm and Novosad, 1990; Nguyen et al., 2014; Osei-Bonsu et al., 2017a), to the properties of the porous medium (Schramm and Mannhardt, 1996; Kovscek and Bertin,

2003; Ma et al., 2012; Gauteplass et al., 2015). The presence of oil is widely accepted to be one of the major deterrents to the performance of foam in porous media (Farajzadeh et al., 2012; Osei-Bonsu et al., 2017a). Oils with low viscosity and carbon chain lengths have been identified to be more detrimental to the stability of foam. Many experiments have revealed that different surfactants exhibit different tolerance to oil and hence potentially different effectiveness in porous media (Andrianov et al., 2012; Osei-Bonsu et al., 2017b).

~~Foam stability in porous media is governed by the limiting capillary pressure (P_e^*), above which foam coalescence becomes significant resulting in increasing the gas fractional flow (Farajzadeh et al., 2015). In other words, when water saturation drops below a limiting water saturation (S_w^*), foam becomes excessively dry (and the lamellae too thin) to survive the imposed capillary pressure. The magnitude of the P_e^* in particular depends on the permeability of the rock (Farajzadeh et al., 2015).~~

The effects of porous media properties such as permeability on foam behaviour have been reported in numerous micromodel and core flooding studies in literature. It has been demonstrated that there is a minimum pressure gradient or critical injection velocity required for foam generation in porous media (Ransohoff and Radke, 1988; Rossen and Gauglitz, 1990; Gauglitz et al., 2002). Gauglitz et al. (2002) showed that the minimum pressure gradient is an inverse function of permeability. In addition to influencing the pressure gradient required for foam generation, permeability affects the apparent viscosity of foam in porous media thus influencing its behaviour and performance as a displacing fluid (Osei-Bonsu et al., 2016).

Although the effects of the presence of textural discontinuity such as permeability contrast on foam flow in porous media have been investigated extensively in the past (Kovscek and Bertin, 2003; Ma et al., 2012), the influence of pore size and grain angularity on foam

generation and propagation in oil saturated porous media have received much less attention. Additionally, the majority of the previous work conducted on the effects of pore geometry has been done using packed sand or core samples in which the geometry and consistency are particularly challenging to control. With the aid of 3D printing technology, we have designed and fabricated porous media with well-defined characteristics in order to investigate the influence of the pore geometry on the dynamics of foam in oil-saturated porous media. The 3D printing technique –allows for fast prototyping and fabrication of customized porous media with consistent and well controlled geometry which cannot be achieved with sandpack or glassbead pack. This has enabled us to visualise and study the effects of pore throat size and grain angularity on foam behaviour and oil displacement by foam in porous media.

2. Experimental Considerations

2.1. Design and fabrication of porous media

Prior to manufacturing the quasi-two-dimensional models used in this study, digital representations of the desired pore throat size distribution and the patterns were designed. 'Rhinoceros' CAD software package for 3D illustrations was used to create the pore networks. The pore network of each model was created from a 'Voronoi' diagram using a random array of points (Sahimi, 2011). Pore throat values were then randomly populated in the model. An algorithm was applied to either straighten or curve the edges of the grains in the model. Four different porous media with well-defined properties were fabricated and used in this study. Figure 1 shows an example of a~~the~~ printed porous medium together with the cross sections of the printed porous media used in the present investigation.

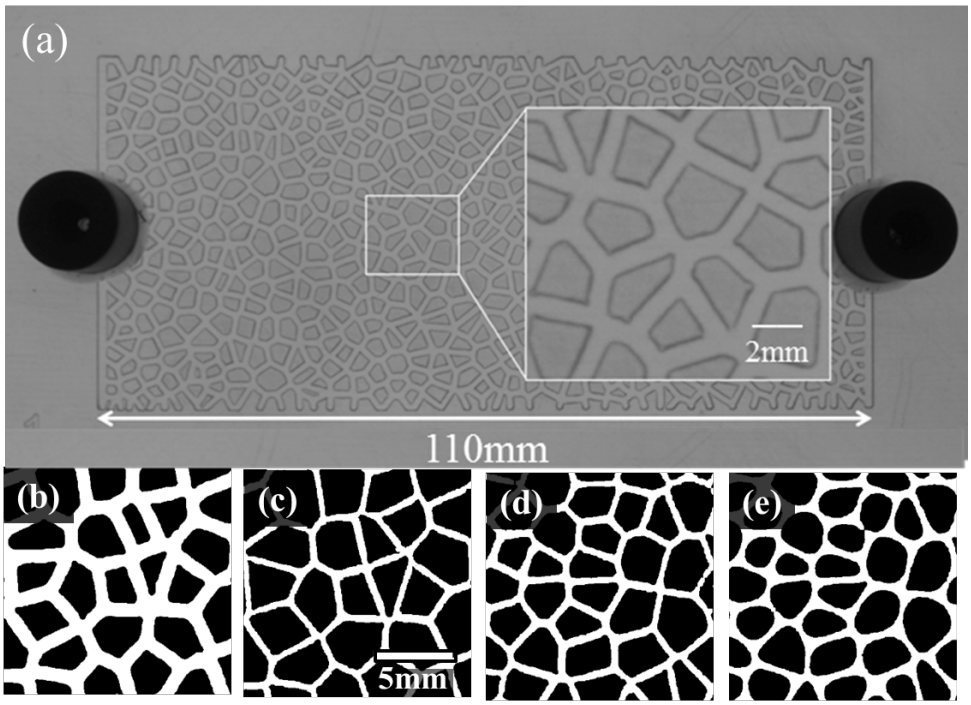

Fig. 1 (a) Top view of one of the printed models with pore-throat-size distribution of 0.8-1.0 mm with angular grains used in our study. (b), (c), (d) and (e) are cross–sections of the printed porous media with pore-throat-size distribution of 0.8-1.0mm and porosity of 45.4% (angular grains; hereafter referred as Model A), 0.3-0.5mm and porosity of 26.2% (angular grains; hereafter referred as Model B), 0.3-0.5 mm and porosity of 30.0% (angular grains; hereafter referred as Model C) and 0.3-0.5mm and porosity of 36.0% (round grains; hereafter referred as Model D), respectively.

The properties of the porous media are provided in Table 1. The dimension of the models was 110 mm x 50 mm and the depth was half the maximum pore throat size in all four models. The spatial distribution of the grains for the models was the same and varied only in pore throat size and grain angularity respectively. The CAD models were converted to stereolithographic (STL) format which were then printed with an acrylic based resin~~material~~ (acrylic oligomer, Tritech, UK) by a high resolution Polyjet 3D printer (Objet 30 pro, Stratasys) (Osei-Bonsu 2017a and 2017b) The printer constructed the models from bottom to

top by depositing and quickly curing thin layers of the liquid resin by UV light. During the printing process, the channels were filled with support material to maintain the shape of the grains and improve the overall precision of the printing. The support material was then washed out using a water jet cleaner after the printing was completed. The top of the printed models were sealed with a glass plate. Two holes of size 1 mm were perforated at the opposite ends of the top glass to allow injection of fluid into and out of the cell.

Table 1. Properties of the printed porous media, number of Voronoi polygons refers to the number of grains in each model.

Model (angularity)	Pore throat size distribution	Number of Voronoi polygons	Circularity	Porosity (%)	Permeability (Darcy)
A (angular)	0.8 – 1.0 mm	660	0.673	45.4	6.3
B (angular)	0.3 - 0.5 mm	660	0.644	26.2	4.7
C (angular)	0.3 - 0.5 mm	990	0.683	32.7	9.5
D (round)	0.3 - 0.5 mm	990	0.748	36.0	10.6

2.2. Fluid properties and experimental procedure

The foaming agent was made from a 1:1 blend of Sodium Dodecyl Sulphate (SDS) (Sigma, UK) and Cocamidopropyl betaine (The Soap Kitchen, UK) (2% wt active content) with a 0.25M NaCl (Sigma, UK) solution. This surfactant combination has been used in previous studies and has shown better tolerance to the presence of oil (i.e. foam films were more stable in the presence of oil) compared to the performance of the surfactants individually (Osei-Bonsu et al., 2015; 2016; 2017a). In this study, foam was generated in-situ by simultaneous injection of the surfactant solution and the gas into the porous medium via separate tubes. The surfactant stream was controlled by a syringe pump (Harvard Apparatus) and the gas by

a mass flow controller (Bronkhorst, UK). Nitrogen (98% purity) was used as the gas phase. Two different ~~types~~ kinds of experiments were conducted in this study. In the first series of experiments, the models were fully saturated with water. Gas and surfactant solution were injected simultaneously to displace the water. In the second ~~type of experiment~~approach, the empty models were initially saturated fully with oil (Isopar V, ~~10.81 × 10^{-3} Pa s~~ - Brenntag, UK, see Table 2). Surfactant solution and gas were then injected simultaneously until all the oil in the models was displaced. A pressure transducer was used to record the pressure during the course of the experiment. The oil phase was stained by a red dye (oil red) to enhance the visual contrast with the displacing phase. The model was thoroughly cleaned with isopropanol and distilled water and dried before conducting the next experiment.

Table 2. Oil properties

Oil	Viscosity (× 10^{-3} Pa s)	Density (g/cm^3)	Surface Tension (mN/m)	Interfacial tension (with surfactant solution (mN/m)
Isopar V	10.81	0.815	25.44	0.130

2.3. Image analysis

Snapshots of the displacement process were captured using a high resolution monochromic camera (Teledyne DALSA Genie) mounted above the model. In order to improve the illumination and the quality of the captured images, a light box was placed beneath the porous media during the experiments. The output images had a resolution of 2560 x 2048 pixels with 8 bit grey levels. A code was developed in MATLAB to segment and distinguish between the oil, grains (solid phase) and foam (gas and surfactant solution). The segmented images were used to quantify the dynamics and efficiency of foam-oil displacement. The segmentation algorithms were similar to the ones described in Shokri et al. (2008, 2012) but

with minor alterations outlined as follows: the areas of the model saturated with oil and foam were distinguished by two main ‘peaks’ in the grey value histogram of each image. The first peak represented oil while the second peak corresponded to foam and the grains. A threshold was assigned to the point on the histogram between the peaks where the derivative of the grey value changed from negative to positive in order to distinguish the two peaks. The grains were then differentiated from foam using the image of the unsaturated model as a reference. The final image was presented in three grey values corresponding to the grains, foam and oil.

3. Results and discussions

This section is laid out as follows. Section 3.1 considers the general influence of pore throat size on the flow properties in porous media. Then Section 3.1.1 and 3.1.2 deal with the dynamics of water and oil displacement by foam respectively. Section 3.2 considers the influence of grain angularity on foam behaviour. Finally section 3.3 discuss the displacement patterns of oil displacement by foam as influenced by pore geometry.

3.1. Effects of pore throat size on foam flow in porous media

For porous media with the same connectivity and topology (e.g. Model A and B), increasing pore throat size (while maintaining the pore-throat aspect ratio, i.e. pore ~~size~~ to throat size,) increases both porosity and permeability of the medium (see Table 1). Consequently, the pressure drop required for fluid displacement decreases according to Darcy’s law. At the pore scale, increasing pore throat size tends to decrease the entry capillary pressure ~~(~~according to Young-Laplace equation:

$$P_c = 2\sigma/r \qquad (1)$$

, $P_e = 2\sigma/r$, where P_c is the entry capillary pressure, σ is the surface/interfacial tension and r is the pore throat radius) and the pressure drop required for fluid mobilization in the throat (given by Poiseuille equation;

$$\Delta P = 8\mu lv/r^2 \quad (2)$$

$\Delta P = 8\mu lv/r^2$ where μ is the viscosity of fluid, l is the length of the pore throat and v is the velocity). As a result of the strength of capillary forces, trapped phase saturation is expected to be higher for porous media with smaller pore throats. In the context of foam, pore throat size can have a crucial effect on the generation and stability of flowing foam in porous media due to its effect on capillary pressure. The following sections will discuss the observed influence of pore geometry on foam behaviour in porous media.

3.1.1. Water displacement by foam

In all the experiments the gas and the surfactant solution were injected at a constant gas fraction of 85% and a total volumetric flowrate of 11.76ml/h (capillary number of 2.75 x 10^{-6} and 5.50 x 10^{-6} for Model A and B, respectively (μ/σ¿ where μ is the apparent viscosity of foam uv is the Ddarcy velocity and σ is the surface tension of the surfactant solution). In order to fully understand the effects of the pore-throat size on foam generation in an oil-saturated model, experiments were first conducted with water as the residing fluid (which may also be considered relevant to foam flow in aquifers). Foam generation and propagation waeres observed immediately after gas and surfactant solution were injected into the models. It was therefore expected that the imposed pressures created by the volumetric flow rate of gas and surfactant solution were above the minimum pressure gradient for foam generation in both models (Gauglitz et al., 2002). Additionally, water had a negligible influence on the stability of the foams hence little minimal bubble coalescence was observed in both cases (Osei – Bonsu et al 2017b). Figure 2a-f show the history of water displacement by foam for Model A and B. It can be observed that, although gas and surfactant solution

were injected as separate phases, stable foam generation occurred almost immediately resulting in a stable, piston – like displacement indicated by the red interface.

Close inspection of the model revealed that the bubbles generated in the porous medium with the larger pore throat size (Model A) were more stable compared to Model B (smaller pore throat) due to higher rate of coalescence in Model B (higher capillary pressure). In addition, some clusters of water were trapped during displacement of water in spite of the higher injection capillary number in Model B. This is ascribed to the presence of continuous gas flowing around such clusters during the early stages of water displacement in Model B due to relatively lower foam stability.

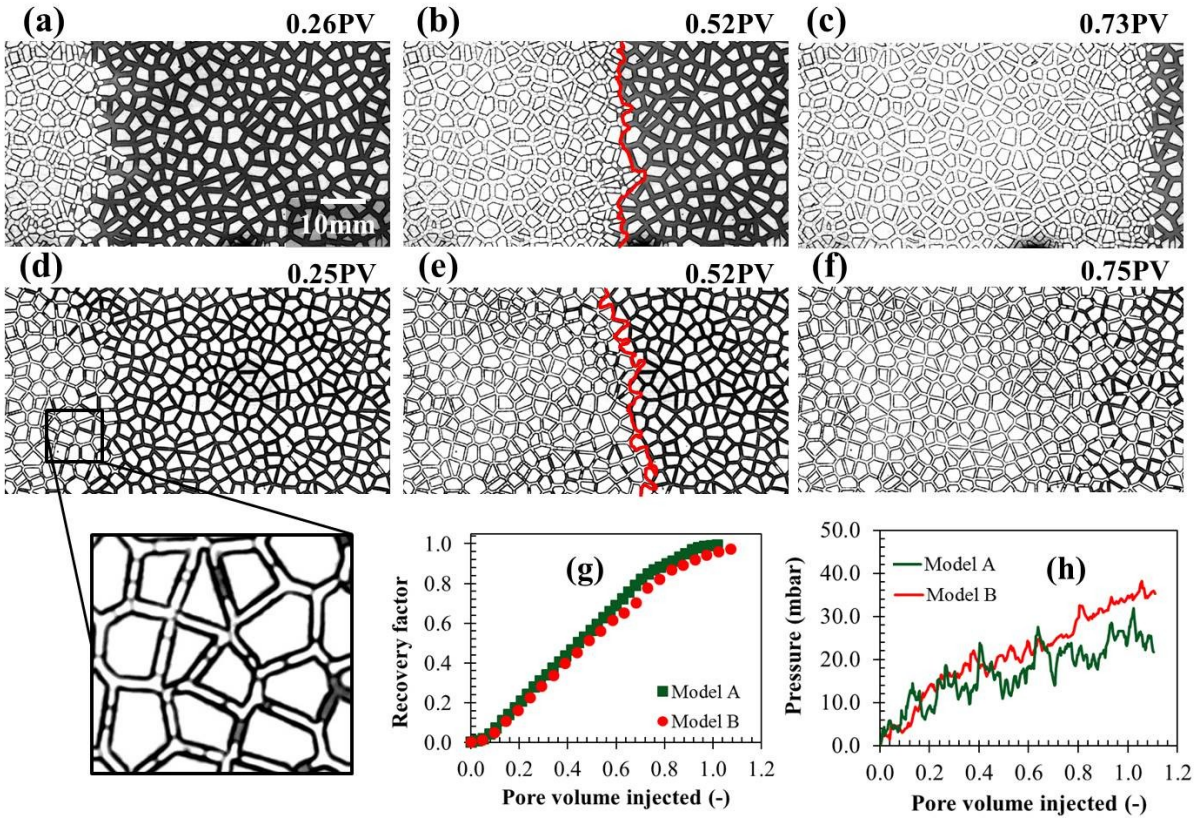

Fig. 2. Water displacement by foam in porous media (a – c) Model A and (d-f) Model B, The red curve represents the interface between foam and water. (g) Recovery of water as a

function of pore volumes of foam (gas and surfactant solution) injected (h) pressure drop across -Model A (green) and Model B (red) during displacement of water by foam.

Irrespective of these ~~effects~~ observed effects of the pore throat size on the dynamics and stability of foam, the water recovery factor, given by the amount of water recovered from the model at that particular time divided by the initial amount of water in the model (i.e. full saturation), was not significantly influenced under these experimental conditions. The recovery of the residing phase in porous media depends on the mobility ratio between the displacing phase and the displaced phase (residing fluid) (Ma et al., 2012). Mobility is defined as the ratio between the relative phase permeability and the phase viscosity. Consequently, increasing the viscosity of the displacing phase decreases the mobility ratio leading to more favourable displacement efficiency. The apparent viscosity of foam can be computed from the steady state pressure drop using Darcy law ~~given by;~~

$$\mu_{app} = \frac{k}{u}\frac{\Delta P}{L} \quad (1)$$

where μ_{app} is the apparent viscosity of foam, k is the permeability, u is the ~~superficial~~Darcy velocity, ΔP is the pressure drop and L the length of the model. The apparent viscosities of foam were 5.07 × 10^{-3} Pa s and 2.21 × 10^{-3} Pa s in both models A and B which are both larger than water, accounting for the stable displacement front indicated by the red curve in Fig 1 (b and e).

3.1.2. Oil displacement by foam

Following the same procedure applied in the case of water displacement, oil displacement experiments were conducted, i.e., the same models were initially filled with the oil followed

by the injection of foam. At the early stages of the injection, co-injection of the surfactant solution and gas resulted in no foam generation thereby allowing the surfactant solution and gas to flow as separate phases in the models even after breakthrough of the gas phase. This is mainly a consequence of the presence of oil in the porous medium which supressed the generation of foam (Osei-Bonsu et al., 2016, 2017a, 2017b). Foam generation in the porous media began after a large fraction of oil had been displaced from the vicinity of the inlet of the model. During the initial phase of foam generation, some of the gas continued to propagate quickly through the porous medium as a separate phase while a fraction of the gas flowed as big bubbles (much larger than the diameter of pores). As fluid injection continued and foam generation progressed, the gas and surfactant solution no longer flowed as separate phases but as successive bubbles (discontinuous gas) due to increase in foam stability. Pore-scale analysis of the displacement process revealed that a smaller pore volume of gas and surfactant was required to initiate the generation of foam in Model A (average pore throat size of 0.9 mm) in the presence of oil (see Figure 3) compared to Model B. According to Young-Laplace equation, the entry capillary pressure for gas to enter a pore throat in Model B is higher than Model A due to its smaller radius. However, in the previous section where the model was saturated with water, foam generation was not significantly influenced by the pore throat size. Analysis of ~~T~~the entry capillary pressure may aid in understanding the reason for this observed phenomenon. Entry capillary pressure in this case was calculated using equation 1, - ❑❑❑ where ❑❑ is the effective radius obtained from the expression for effective diameter, d_e of a rectangular channel (Lenormand 1983);

❑❑❑ ❑ ❑ ❑❑ ❑❑ (4)

where F e is a function approximately equal to 1.0 and x and y are the width and depth or the channel respectively. The entry capillary pressures for gas to invade water and oil filled

models have been provided in Table A1 in the appendix. The entry capillary pressure ~~(2σ/r)~~ for gas to invade the porous media is higher for the water saturated model than for oil saturated model (for Model B it is ~~720~~ 1055 Pa and ~~254~~ 373 Pa, respectively). However, for the case of water displacement the surfactant solution does not have to overcome any capillary pressure to invade a pore throat since water and the surfactant solution are miscible. As a result, there is no barrier for surfactant solution to enter pore throats where foam generation occurs.

Contrariwise, capillarity becomes more significant to foam generation and stability in the case where the model is saturated with oil. In the scenarios considered here, the pressure required for surfactant solution to ~~enter~~ invade a pore throat in Model B is at least twice that required for Model A (1.90 Pa and 0.85 Pa respectively). In addition, the pressure drop required to mobilize oil from a smaller pore throat is higher than for the case of a larger one. The combined effect of these is the higher competition between surfactant solution and oil for pore throats (foam generation sites) as the pore throat size decreases.

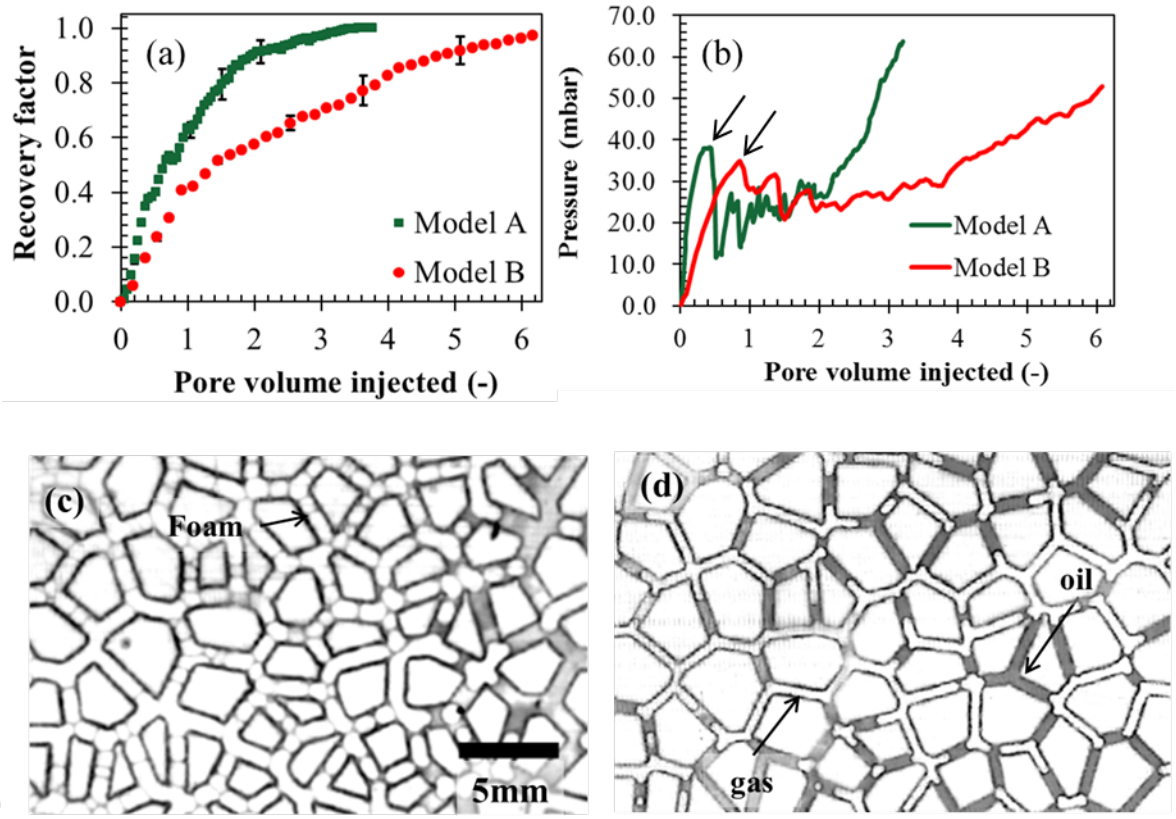

309

310**Fig. 3.** (a) Oil recovery efficiency by foam in porous media labelled as Model A (–average
311pore throat size of 0.9 mm) and Model B (–average pore throat size of 0.4 mm). Each
312experiment was conducted three times and the reported oil recovery curves indicate the
313average behaviour. (b) The pressure profile during oil displacement measured at the inlet of
314the model. Arrows represent breakthrough time. (c) and (d) Typical images of the porous
315media around the inlet after injection of 1 PV of gas and surfactant solution into Model A and
316Model B, respectively.

317The segmented images were used to compute the oil recovery factor during the displacement
318process. Figure 3a shows the oil recovery for Model A and B as a function of total pore
319volume (PV) of the gas and surfactant solution injected. As observed from the figure, the oil
320recovery efficiency by foam reduces as the average pore throat size of the model decreases.
321In the case of Model A, almost all the oil was recovered after injection of 2 PV of foam (gas
322and surfactant solution) whereas in the case of Model B full oil recovery was achieved after

the injection of more than 6 PV. It is worth mentioning that the gas and surfactant solution (not foam) were responsible for oil recovery prior to foam generation as they flowed as separate phases in the models. This may account for the similar oil recovery rates during the injection of the initial 0.2 ~~5~~PV. However, foam generation occurred much sooner in Model A compared to B accounting for the steady increase in oil recovery. As more stable lamellae are formed, the interaction between them increases. Additionally, gas bubbles are trapped in ~~the~~ certain portions of the porous medium retarding the flow of foam and causing the pressure in the model to increase. The faster build up in pressure (gradient of curves in Figure 3b) after gas breakthrough (indicated by the black arrows) as the pore throat size increases, confirms the earlier and higher rate of foam generation and propagation of stable foam (Kovscek and Radke ~~et al.,~~ 1994) in Model A. This is further evidenced by the snap-shots of the inlet region of the pore networks (Figure 3c and d). Figure 3d depicts no foam generation in Model B even after the injection of 1 PV of gas and surfactant solution resulting in the dramatic decrease in the rate of oil recovery after the initial drive of oil by the gas phase. As a consequence of the delay in foam generation, a large fraction of the gas injected into the model followed the already established flow path resulting in little oil recovery. Additionally, trapping of oil during displacement contributes to more coalescence of foam in Model B (Figure 3d) decreasing the strength of foam, further decreasing the rate of oil recovery.

3.2. Effects of grain angularity

In addition to the influence of the pore-throat size on the behaviour of foam in oil saturated porous media, the 3D printing technology enabled us to evaluate the effects of grain angularity on foam flow and generation. Model D was designed such that the positions of the grains were exactly the same as Model C with the exception that the grains were round as

opposed to irregular in the case of the latter. Figure 44 shows the oil displacement efficiency and the pressure profiles for the two models investigated under the same conditions. The oil recovery rate is identical for the two models from the onset of injection until about 1 PV of gas and surfactant solution had been injected. This feature is attributed to the lack of foam generation within this time period. Consequently, as in the previous section, the oil was displaced by mainly gas and surfactant solution flowing through the model as separate phases. Under this displacement condition, the geometry had minimal impact on the recovery of oil. However, after this initial stage, the oil recovery rate increased noticeably in the case of Model D (round grains) compared to Model C (polygonal grains). This is ascribed to the lower entry capillary pressure of the round grains compared to porous media with angular grains ~~because of the larger pore sizes which facilitated earlier foam generation leading to more efficient oil displacement~~(Nourozi Rad and Shokri 2014, Rabbani et al 2016)[33-35].

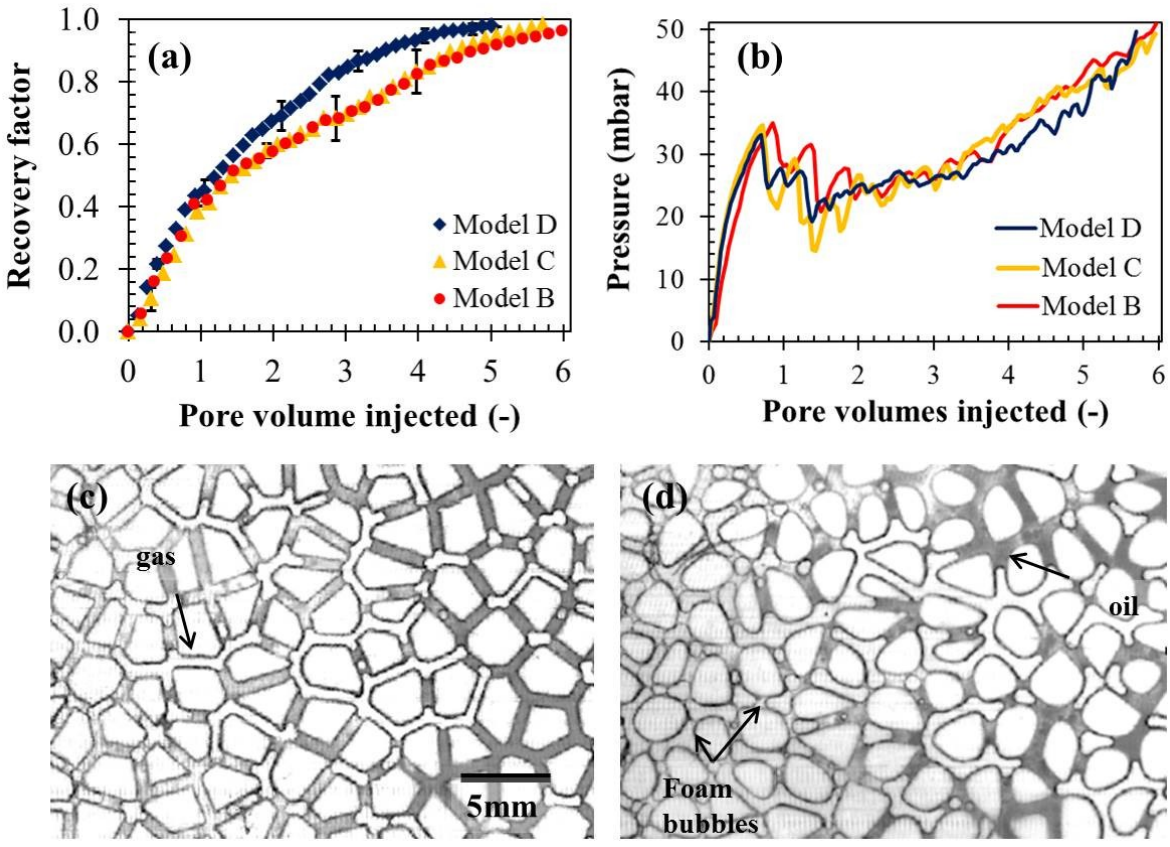

Fig. 4. (a) Oil recovery as a function of pore volume injected in Model B, C (angular grains) and Model D (round grains). (b) Pressure dynamics during oil displacement. (c) and (d) typical images showing the phase distribution around the inlet regions of model C and D respectively after 1.3 PV of surfactant and gas injected into the model. Foam generation in Model D was earlier than Model C.

More importantly, the aspect ratio (ratio of pore to throat) plays a significant role in foam generation by snap-off (Kovscek and Radke 1994, Roof 1970, Nguyen 2000). As shown in the schematic in Figure 5, snap-off mechanism of bubble generation occurs when liquid surrounding the gas phase in a pore flows backward toward the throat as a result of capillary pressure gradient. This gradient is initiated by the differences in curvature and hence pressure between the gas phase in the throat (P_{at}) and the pore (P_{ap}) (subsequently leading to $P_{wp} > P_{wt}$). The flow from the pore to the throat bridges the gas phase in the throat causing the bubble to snap-off (Figure 5b). As the aspect ratio increases (thus as R/r increases) the capillary pressure gradient increases, resulting in higher frequency of bubble generation. In the case of Model D, the roundness of the grains result in larger pores and hence higher aspect ratio (see Figure 5c). Consequently, this mechanism of foam generation is expected to be more dominant in the latter compared to Model C.

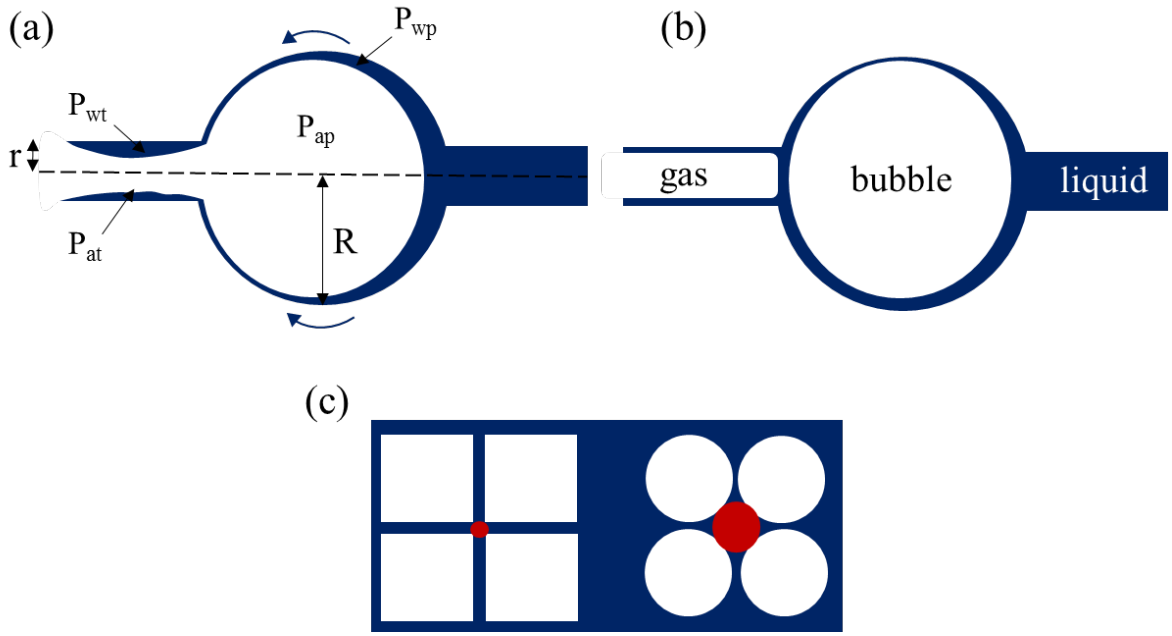

377

378**Fig. 5** Schematic of snap-off mechanism during foam generation in porous media. (a) Liquid
379flows from pore to throat to bridged gas phase due to capillary pressure gradient (b)
380Formation of a new bubble (c) pore geometry created by angular (left) and spherical grains
381(right).

382~~there is a higher pore-throat aspect ratio due to the bigger pore bodies in Model D which~~
383~~provides a higher capillary pressure gradient in the liquid phase (surfactant solution) between~~
384~~the pore body and pore throat (due to smaller curvature in the pore body). This capillary~~
385~~pressure gradient drives surfactant solution from the pore into the pore throat to initiate~~
386~~bubble generation by the snap-off mechanism (Roof, 1970).~~

387

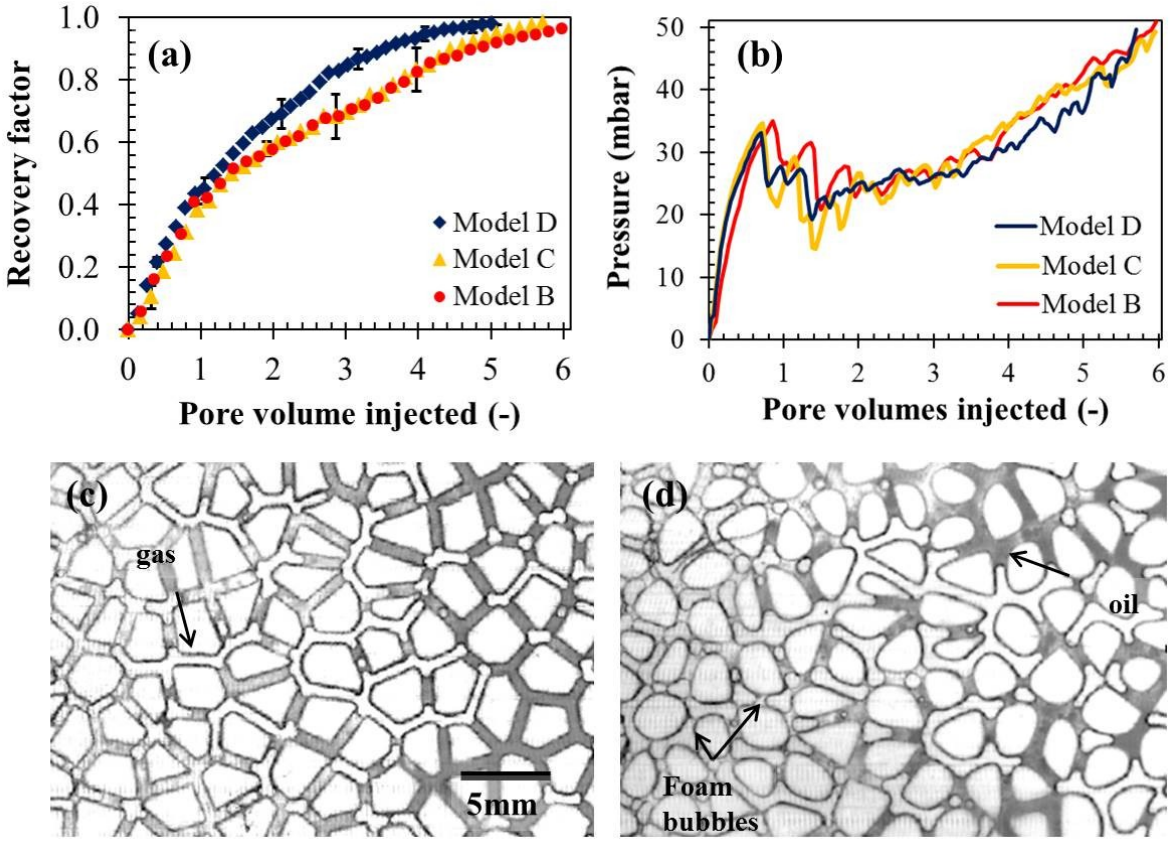

Fig. 4. (a) Oil recovery as a function of pore volume injected in Model B, C (angular grains) and Model D (round grains). (b) Pressure dynamics during oil displacement. (c) and (d) typical images showing the phase distribution around the inlet regions of model C and D respectively after 1.3 PV of surfactant and gas injected into the model. Foam generation in Model D was earlier than Model C.

Unlike Figure 3b, where a glaring difference in the pressure profiles was observed, the variation in the pressure profiles for Model C and D was less due to the similar pore throat size. Nonetheless, careful inspection of Figure 4b shows slightly higher pressure in Model D compared to C particularly (at least) during the initial phase of foam generation (between 1.3PV and 2.5PV). This is indicative of more foam generation which is likewise confirmed by the close up shot of the inlet region depicted in Figure 4c and d.

The effect of permeability on oil recovery was also investigated for porous media of the same pore throat size (Model B and C). In this case, permeability was modified by increasing the number of pores and throat while maintaining the dimensions of the pore throats. Model C consisted of 990 Voronoi polygons (k = 9.5D) whereas Model B was made up of 660 polygons (k = 4.7 D). At the same injection capillary number (5.50 x 10^{-6}), oil recovery factor was not significantly affected by the permeability of the models potentially due to the low range of permeability investigated in this study. The corresponding pressure profiles were also similar in both cases suggesting that under these conditions, the pore throat size and angularity were more influential to the oil displacement by foam than the absolute permeability.

3.3. Dynamics of oil displacement by foam

Figure 6~~5~~ displays snapshots of the phase distributions after 0.5, 1.0 and 1.5 PV of gas and surfactant solution injection in the three models used in our experiments. It can be observed from the snapshots ~~Figure 5 shows~~ that the oil displacement process is influenced by the fingering phenomenon from the very onset of fluid injection into porous media. This is a consequence the lack of foam generation allowing the gas to penetrate the oil in the porous media. As fluid injection progressed, foam began to form in the porous media supressing the fingering effects. Figure 6~~5~~c shows the presence of a stable foam front in the case of Model A (the porous medium with the largest pores) after 1.5PV of injection. However, in the case of Model C and D (Figure 5f and i) fingering phenomena persisted even after 1.5 PV due to the delay in the development of stable foam front. After nearly 2 PV of injection, stable foam fronts developed in the Models C and D (the images are not presented here).

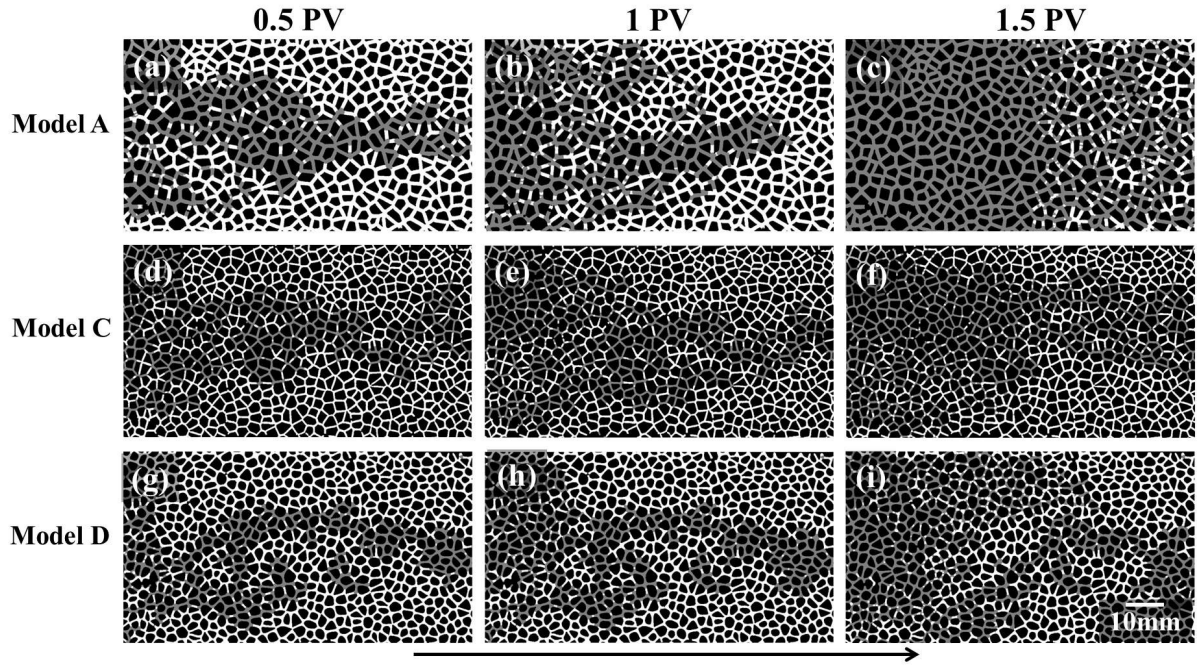

Fig. 65. Dynamics and patterns of oil displacement by foam after the injection of 0.5, 1.0 and 1.5 PV of gas and surfactant solution in Model A (a-c), Model C (d-f) and Model D (g –h). White, grey and black represent oil, foam (surfactant solution and gas) and solid grains respectively.

The development and the evolution of the disconnected oil blobs formed during the displacement process can potentially be influenced by grain angularity and pore throat size as a result of the capillary pressure variation in porous media. Additionally, gas bubbles emerging at the foam front as a result of coalescence travelled rapidly through porous media amplifying the fragmentation of the oil phase. A typical example of this scenario is Figure 5c where disconnected oil blobs are observed ahead of the stable foam front.

Analysis of the disconnected oil blobs as a function of pore volumes injected is presented in Figure 76. The number of these oil fragments as a function of pore volume of fluid injected increased to a maximum (after about 1.2 PV for Model A and about 2.1 PV for Models B, C and D) but declined sharply as the remaining volume of oil in the model gradually decreased.

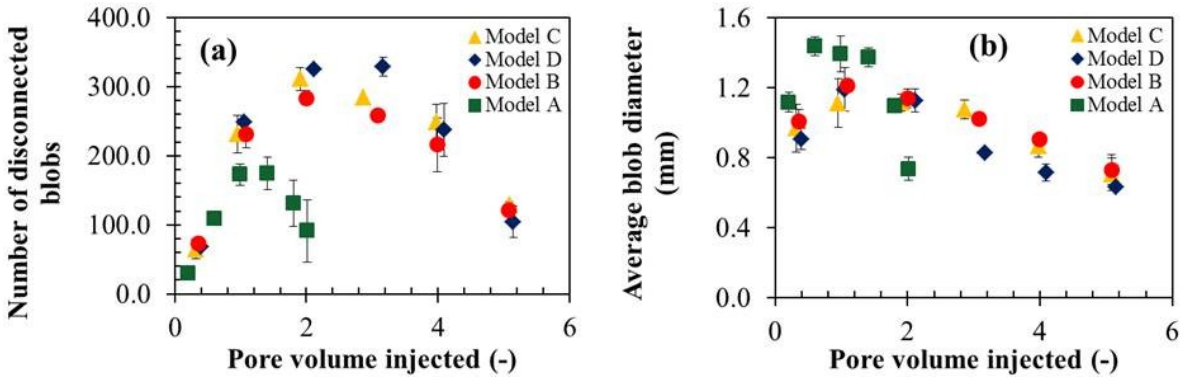

Fig. 7. The influence of the pore geometry on the statistical distribution of disconnected oil blobs during oil displacement by foam. The error bars represent the standard deviations.

Figure 7a shows that as the average pore throat size decreased, the number of isolated oil blobs due to fragmentation increased. The number of disconnected oil blobs were found to be larger in Model B, C and D compared to Model A. A possible reason for this observed result may be the higher capillary pressure associated with smaller pore throats in Model B, C and D compared to Model A. Additionally, the faster development of stable foam front and overall shorter oil recovery time in Model A compared to B and C also contributed to this observation. The average size of the oil blobs resulting from fragmentation was also found to be larger in the case of Model A owing to its larger pore throats (Figure 6b). Still within model A, the average size decreased sharply after about 1.8 PV of foam (surfactant and gas) had been injected as a large fraction of the oil in the model had been displaced at this point. In the case of Model B, C and D, neither the pore geometry nor the number of pores appeared to have a major influence on the fragmentation in the oil phase.

4. Summary and Conclusions

3D printing technology enabled us to fabricate three customised porous networks with well-defined pore geometries. These were used to investigate the influence of average pore throat size and grain angularity on foam generation, propagation and the oil displacement efficiency

in porous media. Foam was generated in-situ following the co-injection of gas and surfactant solution into the porous media. Visualization of oil displacement by foam provided us with an opportunity to describe the effects of the pore geometry and angularity on foam generation and its relationship to the overall oil recovery efficiency. The following conclusions have been deduced from our investigation:

1. Pore geometry plays a crucial role in foam generation and propagation in oil saturated porous media due to its influence on capillary pressure. For porous media with fixed topology, increasing pore throat size decreases capillary pressure of the porous medium which can improve foam generation and stability. In oil saturated models, the influence of pore throat size on generation and propagation of foam is more pronounced due to the additional negative effect of oil on the stability of foam compared to water. Hence the number of pore volumes required for generation and propagation of stable foam was smaller for porous media characterised by bigger pore throats.
2. For porous media with fixed pore throat size distribution, increase in permeability by increasing number of pore throats (and pores) (Model B and C) did not result in any noticeable effect on foam generation and hence oil recovery efficiency.
3. Foam generation is enhanced in porous media with round grains because of high pore-to-throat aspect ratio which results in higher capillary pressure gradient between the fluid at the pore throat and the pore body. This favours foam generation by snap-off mechanism during the initial phase of foam generation.

Although flow in 2D micromodels has several limitations; the most notable being its inability to capture the mixed wetting system encountered in natural occurring porous media, it is nonetheless able to reproduce adequately the underlying physics governing flow in porous media making it a useful tool. With the development in 3D printing technology, we may be able to create porous media with channels of the same order as those occurring in real porous

media and also mimic mixed wetting systems by printing with several materials with different wetting properties.

Appendix

Table A1: The entry capillary pressure is expressed here is the pressure required for gas to invade a water/oil filled pore throat.

Model	Entry Capillary pressure (Pa) (water)	Entry Capillary pressure (Pa) (oil)
Model A	474	165
Model B	1055	373

~~These studies have been carried out in 2D porous media; more complex and intriguing observations are expected in 3D system which offers an avenue for future investigation.~~

Acknowledgements

We would like to acknowledge the UK Engineering and Physical Sciences Research Council (EPSRC) for providing the PhD studentship (EP/L504877/1) for Kofi Osei-Bonsu. Kofi would like to thank Harris Rabbani for the insightful discussions.

References

Andrianov, A., Farajzadeh, R., Mahmoodi Nick, M., Talanana, M., Zitha, P.L.J.: Immiscible Foam for Enhancing Oil Recovery: Bulk and Porous Media Experiments. Ind. Eng. Chem. Res. 51, 2214-2226 (2012).

Binks, B.P., Horozov, T.S.: Aqueous Foams Stabilized Solely by Silica Nanoparticles. Angewandte Chemie. 117, 3788-3791 (2005).

Farajzadeh, R., Andrianov, A., Krastev, R., Hirasaki, G.J., Rossen, W. R.: Foam-oil interaction in porous media: implications for foam assisted enhanced oil recovery. Adv.in Colloid Interf. Sci. 183–184, 1-13 (2012,).

~~Farajzadeh, R., Lotfollahi, M., Eftekhari, A., Rossen, W., Hirasaki, G.: Effect of Permeability on Implicit-Texture Foam Model Parameters and the Limiting Capillary Pressure. Energy & Fuel. 29, 3011–3018 (2015).~~

Gauteplass, J., Chaudhary, K., Kovscek, A.R., Fernø, M.A.: Pore-level Foam Generation and Flow for Mobility Control in Fractured Systems. Colloid and Surfaces A. 468, 184-192 (2015).

Gauglitz, A.P., Friedmann, F., Kam, I.S., Rossen, R.W.: Foam Generation in Homogeneous Porous Media. Chem. Eng. Sci. 57, 4037-4052 (2002).

Grassia, P., Mas-Hernandez, E., Shokri, N., Cox, S.J., Mishuris, G., Rossen, W.R.: Analysis of a model for foam improved oil recovery. J. Fluid Mech. 751, 346-405 (2014).

Hirasaki, G., Lawson, J.: Mechanisms of Foam Flow in Porous Media: Apparent Viscosity in Smooth Capillaries. SPE J. 25, 176-190 (1985).

Hirasaki, G., Miller, C., Szafranski, R., Lawson, J., Akiya, N.: Surfactant/foam process for aquifer remediation. International Symposium on Oilfield Chemistry, Society of Petroleum Engineers, Surfactant/foam process for aquifer remediation (1996).

Jeong, S.W., Corapcioglu, M.Y., Roosevelt, S.E.: Micromodel Study of Surfactant Foam Remediation of Residual Trichloroethylene. Environ. Sci. Tech. 34, 3456-3461 (2000).

Kovscek, A., Bertin, H.: Foam Mobility in Heterogeneous Porous Media. Trans. Porous Med. 52, 17-35 (2003).

Kovscek, A.R., Radke, C.J.: Fundamentals of Foam Transport in Porous Media. Adv. Chem. 242, 115-163 (1994). DOI: 10.1021/ba-1994-0242.ch003.

Lenormand, R., Zarcone, C., and Sarr, A.: "Mechanisms of the Displacement of One Fluid by Another in a Network of C.apillary Ducts," *J. Fluid Mech*. 135, 337-353 (1983)

528Lenormand, R., Touboul, E., Zarcone, C.: Numerical models and experiments on immiscible
529displacements in porous media. J. Fluid Mech., 189, 165-187 (1988).

530Ma, K., Liontas, R., Conn, C.A., Hirasaki, G.J., Biswal, S.L.: Visualization of improved
531sweep with foam in heterogeneous porous media using microfluidics. Soft Matter. 8, 10669-
53210675 (2012).

533Mas-Hernandez, E., Grassia, P., Shokri, N.: Foam improved oil recovery: Foam front
534displacement in the presence of slumping. Colloid Surface A: Physicochem. Eng. Aspects.
535473, 123-132 (2015).

536Nguyen, P., Fadaei, H., Sinton, D.: Pore-Scale Assessment of Nanoparticle-Stabilized CO2
537Foam for Enhanced Oil Recovery. Energy & Fuel. 28, 6221-6227 (2014).

538Norouzi Rad, M., Shokri, N.: Effects of grain angularity on NaCl precipitation in porous
539media during evaporation. Water Resour. Res. 50, 9020-9030 (2014).

540Osei-Bonsu, K., Shokri, N., Grassia., P.: Fundamental investigation of foam flow in a liquid-
541filled Hele-Shaw cell. J. Colloid Interface Sci. 462, 288-296 (2016).

542Osei-Bonsu, K., Grassia, P., Shokri, N.: Investigation of foam flow in a 3D printed porous
543medium in the presence of oil. J. Colloid Inter. Sci. 490, 850–858 (2017a).

544Osei-Bonsu, K., Grassia, P., Shokri, N.: Relationship between bulk foam stability, surfactant
545formulation and oil displacement efficiency in porous media. Fuel. 203, 403–410 (2017b).

546Osei-Bonsu, K., Shokri, N., Grassia., P.: ~~Surfactant dependent f~~Foam stability in the presence
547and absence of hydrocarbons: From bubble- to bulk-scale. Colloid Surface A. 481, 514–526
548(2015).

549Payatakes, A.: Dynamics of Oil Ganglia During Immiscible Displacement in Water-Wet
550Porous Media. Ann. Rev. Fluid Mech. 14, 365-393 (1982).

551Pennell, K.D., Pope, G.A., Abriola, L.M.: Influence of Viscous and Buoyancy Forces on the
552Mobilization of Residual Tetrachloroethylene during Surfactant Flushing. Environ. Sci.
553Technol. 30, 1328-1335 (1996).

554Rabbani, H.S., Joekar-Niasar, V., Shokri, N.: Effects of intermediate wettability on entry
555capillary pressure in angular pores. J. Colloid Interf. Sci. 473, 34-43 (2016).

Ransohoff, T., Radke, C.: Mechanisms of Foam Generation in Glass-Bead Packs. SPE Reservoir Eng. 3, 573-585 (1988).

Roof, J.: Snap-off of Oil Droplets in Water-Wet Pores. SPE J. 10, 85-90 (1970).

Rossen, W.R., Gauglitz, P.A.: Percolation theory of creation and mobilization of foams in porous media. AIChE J. 36, 1176-1188 (1990).

Sahimi, M.: Flow and Transport in Porous Media and Fractured Rock: From Classical Methods to Modern Approaches. 733 pp., Wiley- VCH Publishers, Weinheim, Germany (2011).

Schramm, L.L., Mannhardt, K.: The effect of wettability on foam sensitivity to crude oil in porous media. J. Petrol. Sci. Eng. 15, 101-113 (1996).

Schramm, L.L., Novosad, J.J.: Micro-visualization of foam interactions with a crude oil. Colloids and Surfaces. 46, 21-43 (1990).

Schramm, L.L., Wassmuth, F.: Foams: Basic Principles. Adv. Chem. 242, 3-45 (1994). DOI: 10.1021/ba-1994-0242.ch001.

Shokri, N., Lehmann, P., Vontobel, P., Or, D.: Drying front and water content dynamics during evaporation from sand delineated by neutron radiography. Water Resour Res. 44, W06418 (2008).

Shokri, N., Sahimi, M., Or, D.: Morphology, propagation dynamics and scaling characteristics of drying fronts in porous media. Geophys Res. Lett. 39, L09401 (2012).

Zeng, Y., Ma, K., Farajzadeh, R., Puerto, M., Biswal, S.L., Hirasaki, G.J.: Effect of Surfactant Partitioning Between Gaseous Phase and Aqueous Phase on CO2CO2 Foam Transport for Enhanced Oil Recovery. Trans. Porous Med. 114(3), 777-793 (2016).